Talanta 130 (2014) 400–407

Contents lists available at ScienceDirect

Talanta

journal homepage: www.elsevier.com/locate/talanta

Characterization of a new mobility separation tool: HRIMS as differential mobility analyzer

Marcos Bouza [a], Silvia López-Vidal [c], Jorge Pisonero [b], Nerea Bordel [b,*], Rosario Pereiro [a,*], Alfredo Sanz-Medel [a]

[a] Department of Physical and Analytical Chemistry, Faculty of Chemistry, University of Oviedo, 33006 Oviedo, Spain
[b] Department of Physics, Faculty of Science, University of Oviedo, 33007 Oviedo, Spain
[c] RAMEM, 28027 Madrid, Spain

ARTICLE INFO

Article history:
Received 16 June 2014
Accepted 30 June 2014
Available online 15 July 2014

Keywords:
Differential mobility analysis
Volatile organic compounds
Photoionization
Water cluster identification

ABSTRACT

High resolution ion mobility spectrometer (HRIMS) is a new instrument that uses parallel plate Differential Mobility Analysis as principle of separation. Gas phase analysis of volatile organic compounds (VOCs) has been performed for the characterization of this new mobility system using an UV-lamp for ionization. Studies of the effect of temperature and the presence of a desiccant are detailed. Identification of the different peaks obtained with an electrometer was successfully carried out for a group of alcohols, aromatic compounds and ketones (ethanol, 1-propanol, isopropanol, 1-butanol, 1-pentanol, 1-heptanol, acetone, 2-butanone, 2-pentanone, 2-octanone, benzene, toluene, xylene and bromobenzene) following a modified Millikan equation. Moreover, the investigation of the discrimination capabilities within the different VOCs families as well as the mobility dependence with molecular mass was successfully achieved.

1. Introduction

Ion mobility spectrometry is used to classify chemical substances based on the velocity of gas-phase ions in an electric field [1]. Ion mobility was initially conceived for the detection of volatile organic compounds (VOCs), chemical warfare agents and explosives [2]; however, innovative applications have been appearing along the last years in areas as diverse as proteomics [3] or environmental analysis [4,5]. There are three main approaches using ion mobility in gas phase as the separation principle that are typically known as Ion Mobility Spectrometry (IMS), Differential Mobility Spectrometry (DMS) and Differential Mobility Analysis (DMA). In conventional IMS, which is the more mature technology, ions are injected into a drift tube using a shutter grid that allows a pulsed sampling. Ions enter then an electric field region where their velocity will depend on their mass, size, shape and charge state [2]. An important drawback of this technique is the need of a pulsed sampling mode. In order to overcome this limitation, other instrumental strategies for ion mobility have been introduced including DMS [6] or Field Asymmetric Ion Mobility Spectrometry (FAIMS) and DMA [7]. In the case of DMA, the separation of the chemical substances is performed in terms of space, instead of time [8]. Parallel plates DMA design is one of the most recent and less studied strategies that use ion mobility as separation mechanism for gas phase analysis. DMA has been traditionally used to measure the particle size distribution of aerosols in the submicron range (<1 μm) as those emitted in combustion processes and atmospheric aerosols [9]. The modern rise of nanotechnology has prompted a further development of DMAs for nanoparticles (1–100 nm) classification [10].

Ion mobility instruments usually resort to simple and robust components for atmospheric pressure measurements. For instance, typical ion sources are based on radioactivity, photoionization and corona discharges. In particular, photoionization is considered a good choice due to its robustness and easy handling, although it has a limited ionization potential. In relation to the detectors, ion counting devices (e.g. Faraday cups) are typically employed for ion mobility measurements. As this type of detectors just measure the current created when a beam of charged particles collide with the metallic surface of the device, the identification of the ions must be carried out using chemical standards or mathematical approximations.

For mobility analysis, the analyte ions are introduced at ambient gas pressure into a voltage gradient or electric field (E). Thus, ions attain a velocity (u) that is proportional to the electric field strength (Eq. (1))

$$u = ZE \tag{1}$$

The proportionality coefficient, Z, is termed the "mobility coefficient" of the ion. The electrical mobility allows the characterization of the molecular size [11,12]. For the case of particles much larger than atomic dimensions although much smaller than the gas mean free path, Z is an inverse measure of the cross-sectional area of the particle, whenever these molecules are

* Corresponding authors.
E-mail address: bordel@uniovi.es (N. Bordel).

http://dx.doi.org/10.1016/j.talanta.2014.06.073
0039-9140/

considered as spherical particles. For instance, Tammet [13] used an approximation of the Millikan law, collected in Eq. (2), to identify different molecules as a function of their size using DMA analysis

$$Z = 0.441\frac{ze(kT/m)^{1/2}}{p(d_\rho + d_0)^2} \quad (2)$$

where p, T and m are the pressure, absolute temperature and molecular-mass of the background gas (air), respectively. k is the Boltzmann's constant, z is the ion charge, and d_ρ and d_o are the molecule diameter and the gas molecules diameter of the surrounding particles (d_o=0.3 nm [14,15]). Based on this approach and on the reactivity of the species, which is related to the ionization source, analyte molecules can be identified from the mobility spectrum. Alternatively, ion mobility spectrometers can also be coupled on-line with powerful detectors (e.g. mass spectrometers [16]) to further facilitate such identifications of the different species.

The aim of this work is to study the influence of different experimental parameters of a new DMA prototype, named High Resolution Ion Mobility Spectrometer (HRIMS) [17], in the resulting mobility spectra. In addition, it is investigated the possible identification of the peaks appearing in the spectra and the characterization of the mobilities originated during practical analysis of different VOCs.

2. Experimental

2.1. Instrumentation

The differential mobility analyzer used in these studies, the HRIMS, is a mobility prototype developed by RAMEM under its trademark IONER (www.ioner.eu) [7]. A schematic of the DMA structure is shown in Fig. 1a. It is a closed-circuit rectangular duct, in which a sheath gas (usually air) flow is generated with a compressor. This flow is measured in a Venturi type flowmeter that is placed upstream. A heater is also located in the circuit allowing the control of the sheath gas temperature. Pressure and temperature are measured in two points of the circuit as can be seen in Fig. 1a. The humidity is reduced by using desiccant particles placed in a container included in the gas sheath circuit. A diagram of the separation (classification) zone is shown in Fig. 1b. As can be seen, a gas flow containing the sample ionized species enters the DMA through a slit and joins a particle-free orthogonal air sheath, which flows between two parallel plate electrodes. The ions migrate from one electrode to the other under the action of the uniform electric field established by applying a voltage between the plates. Only the ions of a given polarity and electrical mobility will leave the DMA through a slit in the outer electrode. Usually the DMA operates in conditions such that the ion injection and the ion extraction flow rates are equal. Mobility of the classified ions (Z) is a function of the operating conditions and the geometry of the working region of the DMA as shown in Eq. (3) [18]

$$Z = \frac{Ql_y}{Vl_x l_z} \quad (3)$$

where Q is the sheath flow rate, V is the applied voltage, l_x is the axial distance from the ion inlet slit to the ion outlet slit, l_y is the separation between the electrodes, and l_z is the width (in the direction perpendicular to the plane) of the working region.

The ions from the sample continuously enter the DMA, where they are classified by varying the voltage applied to the outer electrode. In particular, the DMA classifies ions with mobilities in the range between 0.6 and 4 $cm^2\,V^{-1}\,s^{-1}$. The ion outlet slit is located downstream; the Faraday cup collects the mobility classified ions and the current is measured with an electrometer (Electrometer EL-5020, Ramem S.A, Madrid, Spain). RAMEM's parallel plate DMA's are considered to have advantages with respect to cylindrical DMAs regarding the transmission of ions due to lower losses in this simpler geometry.

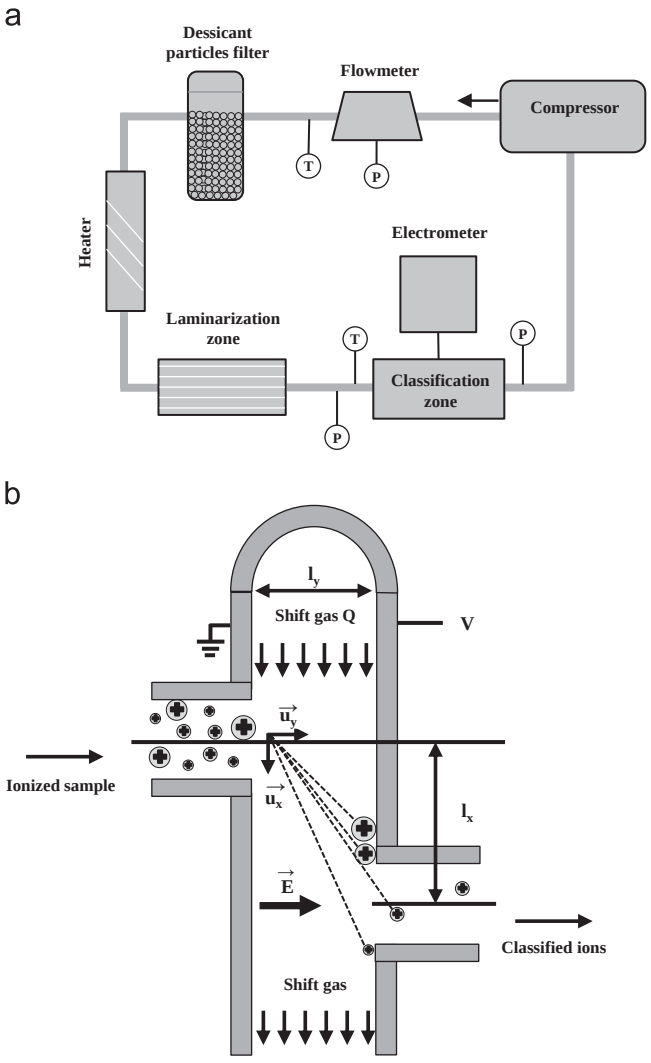

Fig. 1. (a) Schematic representation of the principal components presents in the HRIMS (T: thermocouple and P: pressure gauge). (b) Separation zone of parallel plate DMA (HRIMS).

The technical specifications of the equipment are collected in Table 1. Photoionization (UV-lamp of 10.6 eV) has been used as ionization source all along this work. In order to investigate the behaviour of VOCs at different analysis conditions, the analyte was placed in a flask of 250 mL filled with nitrogen (99.999%, Air Liquide) at room temperature and ambient pressure. Before the beginning of the measurements, the aspiration pump was activated and the mixture of nitrogen with a VOC was introduced in the ionization zone, helped by the vapour pressure of the VOC (all VOCs used are volatile at ambient temperature).

2.2. Chemicals

Three groups of VOCs (alcohols, ketones and aromatic compounds) (Sigma-Aldrich) were selected to characterize the HRIMS. Table 2 collects the specific compounds employed (suitable for the aspiration sampling system used) with different functional groups,

Table 1
HRIMS technical characteristics.

Measuring principle	Ion mobility
Mobility range	0.06–4 $cm^2 V^{-1} s^{-1}$
Sampling	Direct or with membrane
Detection	Electrical current
Dynamic range	4 decades
Sample flow rate	From 0.1 to 1.5 $Lmin^{-1}$
Sheath flow rate	From 170 to 900 $Lmin^{-1}$
Voltage	Up to 7.5 kV
Resolving power (cm^2/V s)	50
Ion polarity	Positive/negative
Measurement time lapse	1–5 min
Power	110–220 VAC 50–60 Hz
Max. Consumption	700 W
Working temp. range	5–90 °C
Storage temp. range	−20–60 °C
Humidity working range	5–80%
Weight	25 Kg
Dimensions:	90 × 40 × 40 cm^3

Table 2
Molecular mass of the different compounds used in the present work. Dimethyl methylphosphonate (DMMP) is highligthed in the table as the mobility standard used during this work.

Compound	Molecular weight
Ethanol	46.07
Acetone	58.08
1-propanol	60.01
Isopropanol	60.01
2-butanone	72.11
1-butanol	74.12
Benzene	78.11
2-pentanone	86.13
1-pentanol	88.15
Toluene	92.14
Xylene	106.16
1-heptanol	116.88
DIMETHYL METHYLPHOSPHONATE	124.08
2-octanone	128.21
Br-benzene	157.02

Table 3
Optimal conditions analysis.

Shift gas	Air
Sample dragging gas	Nitrogen
Shift flow	150 l/min
Gas sheath temperature	90 °C
Sample flow	1 l/min
Extraction flow	1.2 l/min
Scan voltage	500–4500 V

sizes and degree of saturation. Moreover, dimethyl methylphosphonate (DMMP) (Sigma-Aldrich) was used as mobility standard.

Different desiccants were investigated: drierite (Sigma-Aldrich), molecular sieve of 4 Å diameter pore (Sigma-Aldrich) and silica gel (Servoquimia). Nitrogen (99.999%) from Air-Liquide was used as carrier gas.

3. Results and discussion

3.1. Optimization of analysis conditions of HRIMS

An optimization of the parameters that influence the signal intensity and the mobility value in this new instrumentation was first carried out. The analytes used for these optimization studies are recorded in Table 2. Additionally, Table 3 collects the working gases and the flow rates selected as well as the scan voltage applied. These values were selected after a univariant optimization focused on maximizing the signals detected. The studies for the most critical parameters, gas temperature and humidity [19,20], are described below to show their role on the mobility spectra and on the species created during the ionization processes.

3.1.1. Temperature

Gas temperature influences the peak shapes (width, position and height) and the resolution of the mobility separations [21,22] via: (1) ion chemistry during the ionization at atmospheric pressure since the degree of clustering varies with temperature, and (2) drift behaviour of ions through the drift tube because differences in gas density gives rise to changes in the mean free path of ions and therefore in the collision rates.

In this work, we studied the ion mobility spectra obtained for different selected VOCs using the HRIMS set-up at four gas temperatures (30, 50, 70 and 90 °C). Fig. 2 shows the current intensities measured *versus* $1/Z_0$ (being $Z_0=Z$ (273/T)(P/760) reduced mobility) for acetone (Fig. 2a) and 1-propanol (Fig. 2b). Results reveal more intense mobility spectra at higher gas temperatures with analyte peak features much better defined, as well as shifts in the mobility peaks. In particular, the registered intensity at any mobility is higher at 90 ºC for all VOCs analysed. Shifts of the mobility peaks are only observed at higher temperatures (> 70 °C). In the case of 1-propanol (Fig. 2b) the mobility spectra show peak displacements as a function of the gas temperature. For example, at 30 °C, the predominant peaks are observed at the highest mobility; at 50 °C, peaks with similar intensities are detected in the mobility range under study; and at 70 °C, the spectrum is shifted towards lower mobility. In general terms, a slight shifting towards lower mobilities with increasing temperature seems to occur for all the compounds under study. Finally, new peaks may appear at higher temperatures (*i.e.* peaks barely detectable at low temperature, became more intense and better resolved by increasing the temperature).

3.1.2. Humidity

The humidity in the HRIMS circuit is a key factor that governs the actual species generated during the ionization processes. Humidity is inversely related to the gas temperature in the instrument (the design of the present prototype allows increasing the temperature up to 90 °C). As 90 °C is not enough to eliminate existing humidity, some desiccants were also used to reduce the excess of ambient water present in the gas sheath circuit (Fig.1a). For instance, drierite, silica gel and molecular sieve were investigated. Differences between the mobility spectra obtained for the different VOCs with and without desiccant were significant, while variations among the spectra obtained using three different desiccants were irrelevant. Consequently, drierite was finally chosen because of its easy regeneration and the drastic colour changes of dry/wet states of drierite.

As a typical illustration, Fig. 3 shows two spectra of ethanol, measured under the selected operational conditions, with and without drierite at 90 °C. As can be seen, peaks with similar shape and mobility (1.60, 0.80 and 0.63 Vs/cm^2) in both spectra were apparent. In addition, the presence of the desiccant (and so the decrease of the humidity in the instrument's circuit) gave rise to new peaks (as those observed between 1.20 and 1.60 Vs/cm^2) that cannot be observed without drierite.

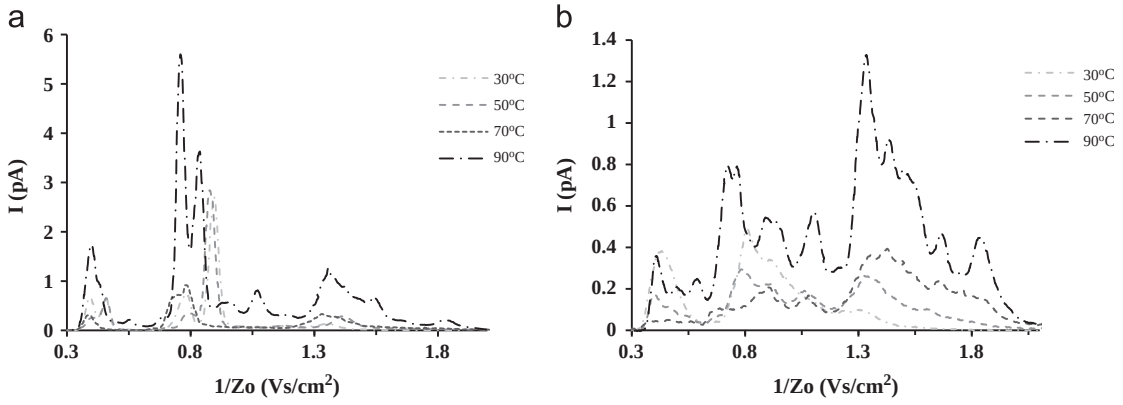

Fig. 2. Influence of different temperatures (30, 50, 70, 90 °C) in the mobility spectrum of: (a) acetone and (b) 1-propanol.

3.2. Peak identification

The identification of the different peaks found in the mobility spectra was investigated following the criteria used for Ku et al [23]. Even if the two ion sources (electrospray in the Ku et al. work, and UV in this one) are different (that is, ionization mechanisms can be different), both generate ions without fragmentation (additionally, in the case of electrospray, there is also the possibility of multiple charges formation).

Photoionization may be used as a means of ionizing neutral molecules at ambient pressure air. UV lamps emit photons after the electrical excitation of the gases filling the UV lamp. Photons energy lies in a range between 9.5 and 10.6 eV, high enough to ionize most of the common organic compounds (with ionization potentials between 7 and 10 eV). The formation of positive ions by such photon absorption has been described as direct ionization or as proton transfer as shown in Eqs. (4–9)

$$h\upsilon + M \rightarrow M^{\bullet +} + e^- \quad (4)$$

$$M^{\bullet +} + M \rightarrow [M+H]^+ + [M-H]^{\bullet} \quad (5)$$

$$h\upsilon + H_2O \rightarrow H_2O^{\bullet +} + e^- \quad (6)$$

$$H_2O^{\bullet +} + H_2O \quad (or\ a\ neutral\ as\ H\ source) \rightarrow [H_2O+H]^+ + [H_2O+H]^{\bullet} \quad (7)$$

$$M + (H_2O)_n\ H^+ \rightarrow (H_2O)_{n-x}\ MH^+ + xH_2O \quad (8)$$

$$(H_2O)_m MH^+ + M \rightarrow (H_2O)_{m-y} M_n H^+ + yH_2O \quad (9)$$

where $h\upsilon$ is the photon energy, M the neutral molecule and H^+ a proton. M^+ is the most common species produced. The exact mechanism of ion formation in air at ambient pressure should be considered as incompletely understood for compounds of high proton affinity or compounds for which protons can be released [3].

Once the VOC analytes are introduced in the ionization region they will be ionized following the process indicated in Eq. (4). In addition, these analyte ions can interact with hydration clusters ($H[H_2O]_n^+$, present in the sheath gas due to the humidity, producing $MH[H_2O]_n^+$ or M_mH^+). The instrument has been calibrated using the two known mobility peaks of the DMMP [24]: measurements carried out with our instrument present two peaks at 2.544 cm^2/Vs (monomer) and 1.358 cm^2/Vs (dimer).

Fig. 4 collects the registered mobility spectra with peak assignments for three compounds (2-butanone, benzene and 1-propanol, respectively) of different families of VOCs (ketones, aromatic compounds and alcohols) selected. To carry out peak assignments we assumed that the second ionization potential for these VOCs is superior to that provided by the photoionization source (10.6 eV). Therefore, as can be seen in Fig. 4, the different peaks identified

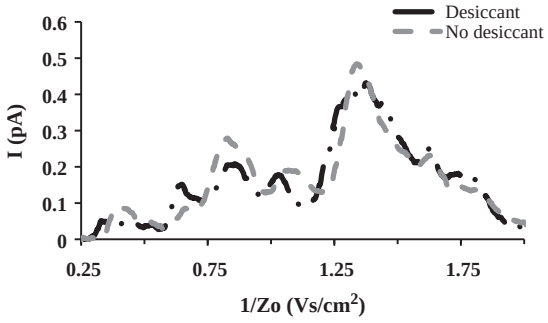

Fig. 3. Mobility spectra for ethanol with or without desiccant in the HRIMS circuit.

with this approximation are mono-charged ions with different degrees of hydration or coordination, being also possible to observe aggregates of the analyte in most of the molecules studied. For these assignments we considered that, according to Ku et al., the behaviour $m_p^{1/3} \sim (z/Z)^{1/2}$ (where m_p is the ion mass) can be assumed for spherical ions. This dependence comes from Eq. (2), where it is clear that $(z/Z)^{1/2}$ is proportional to d_p (d_p is the ion diameter), together with the relation m_p–d_p^3 valid for the spherical ion approximation.

Fig. 4a shows an example, for 2-butanone, of the peak identification, as investigated for the different ketones under study. According to the species identification carried out in this work, the different ketones have a multiple peak spectra where the different ions identified correspond to species with different number of molecules of the ketone analysed; also when the size of the ketones increase the number of neutrals that could be coordinated to the MH^+ decrease as a consequence of the steric hindrance. In all the compounds of the family there a first peak that could corresponds to the M^+ or to the MH^+; according to bibliography [3], during the ionization process ketones form preferentially MH^+ instead of M^+(expected with photoionization).

On the other hand, the analysed aromatic compounds show other type of ion species following the approximation. Aromatic compounds are coordinated with a water cluster ($H(H_2O)_4^+$) forming $MH(H_2O)_4^+$; according to the bibliography, this water cluster in a tretameric form is stable and it favours the coordination of the π-cloud of the aromatic compounds [25]. The other species, identified with the Millikan's approximation, are the consequence of neutral aromatics molecules coordinated to this ion. The mobility peaks detected for benzene (Fig. 4b), toluene, xylene and Br-benzene have the same mobilities except in the case of the peak assignment for the aromatic compounds with the water clusters tetramer. During the classification process the difference in mobility for the compounds are not so noticeable to clearly distinguish the peaks detected for the different compounds.

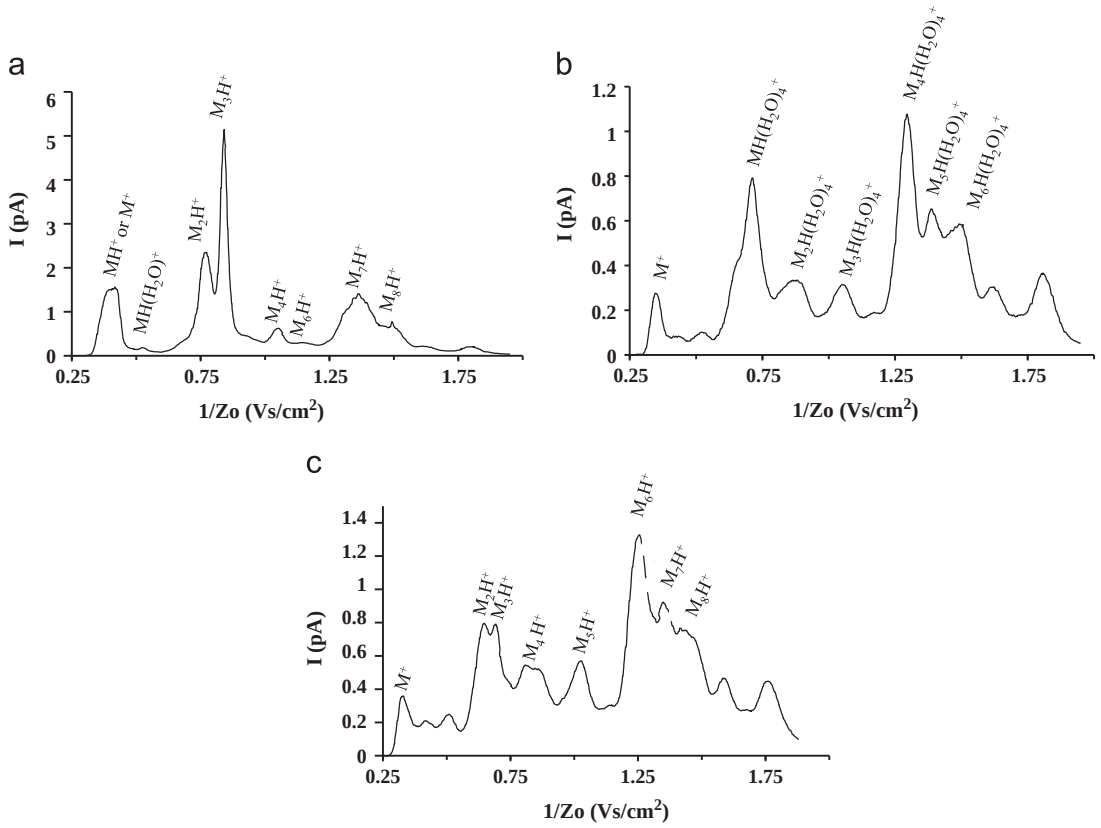

Fig. 4. Peak identification of the different mobility spectra for different VOCs with the ions generated during the ionization process with an UV-lamp using optimized conditions: (a) 2-butanone ions, (b) benzene ions and (c) 1-propanol ions.

Fig. 4c illustrates the behaviour of alcohols. The proton affinity of alcohols lies midway between ketones and aromatic compounds and, as can be seen, the spectra for alcohols show similarities with those acquired for aromatic compounds (i.e. poor resolved peaks), but the pattern of the spectra is different. In this case, the alcohols present the formations of aggregates according to the approximation used during the present work.

As a complementary tool, Chem3D was used to simulate the molecular dynamics of the aggregates. MM2 force field package was employed for the calculation [26]. The ions involved in the simulation were distributed randomly, but close enough to each other easing the Coulombic attractions. The first step of the simulation was to find the energy-minimum configuration and, then, the simulation of the interactions was carried out; afterwards, volume calculations were performed. These volumes were used for comparison with the diameter obtained by the approximation employed in the present work. The different diameters present deviations minor than a 6% for all the compounds studied.

As an example of the assignments carried out in this work, Fig. 5 shows the plot $m^{1/3}$ *versus* $(z/Z_0)^{1/2}$ for 2-butanone, benzene and 1-propanol species, respectively. As can be seen, the data fits to linear functions with good correlation coefficients. Table 4 collects the peak identification, the corresponding mass and the $1/Z_0$ (Z and Z_0 are proportional) values for the different peaks in the spectra for all the compounds under study.

3.3. HRIMS discriminating capabilities for different VOCs' families

Fig. 6 presents the ketones, aromatic compounds and alcohols mobility spectra at optimized conditions. Again, the different compounds were analysed independently. While aromatic compounds and alcohols (Figs. 6b and 6c, respectively) showed quite similar type of spectra, ketones (Fig. 6a) had better resolved peaks exhibiting higher intensity as well.

The observed mobility spectra of the studied ketones (acetone, 2-butanone, 2-pentanone and 2-octanone) show three regions: around 0.3 Vs/cm^2, 0.8 Vs/cm^2 and 1.4 Vs/cm^2. As it was identified above, these regions correspond to three different sizes of molecules. Two peaks are observed for the ketones (Fig. 6a) around 0.8 Vs/cm^2. These peaks correspond to the dimer (M_2H^+) and to the trimer (M_3H^+). The four ketones under analysis could be distinguished using any of those two peaks, considering that the reduced mobility of the molecules were different. As it can be observed in Fig. 6a, the lighter compound had the lowest inverse of reduced mobility (the biggest reduced mobility).

The spectra for aromatic compounds and alcohols (as shown in Fig. 6b and c) are more complex and, so, a good separation between the different peaks became more difficult. Regarding the aromatic compounds, it is worth to highlight that the spectral region for $MH(H_2O)_4^+$ (region inside the box in Fig. 6b) could be used to identify the four aromatic compounds, although the resolution of our instrument at this point does not allow a proper peak separation. On the other hand, the peaks highlighted in the case of the alcohols (M_2H^+–M_3H^+ in Fig. 6c) represent a region that could allow the differentiation between the six alcohols under study. In any case, multivariate analysis tools that take into account the characteristic peaks should be used to identify mixtures of the different investigated compounds.

3.4. Mobility dependence with molecular mass

Trying to deepen in the HRIMS discriminating capabilities, we have investigated the reduced mobilities measured for some species of the different VOCs under study (Fig. 7). Fig. 7a collects the mobility for three types of species MH^+ or M^+, M_3H^+ and

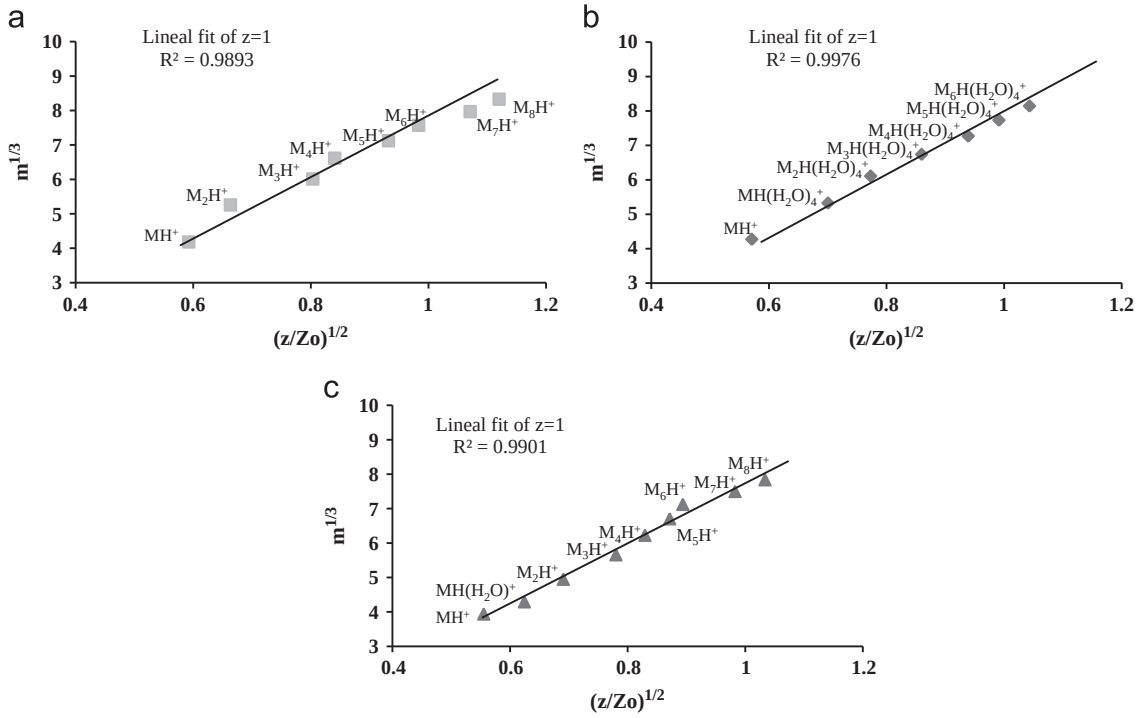

Fig. 5. Linear correlation graph for the three representative compounds. Graph represents $(z/Zo)^{1/2}$ *versus* $m^{1/3}$ for: (a) 2-butanone ions, (b) benzene ions, and (c) 1-propanol ions.

Table 4
Ion peak identification of the different water clusters using the Millikan approximation for the VOCs under study.

Compounds	Acetone		2-butanone		2-pentanone		2-octanone		Compound	Benzene		Toluene		Xylene		Br-Benzene	
	mass (amu)	1/Zo (Vs/cm^2)	mass (amu)	1/Zo (Vs/cm^2)	mass (amu)	1/Zo (Vs/cm^2)	mass (amu)	1/Zo (Vs/cm^2)		mass (amu)	1/Zo (Vs/cm^2)	mass (amu)	1/Zo (Vs/cm^2)	mass (amu)	1/Zo (Vs/cm^2)	mass (amu)	1/Zo (Vs/cm^2)
									M^+	78.11	0.347						
MH^+ or M^+	58.08	0.365	72.11	0.418	86.13	0.437	128.21	0.748									
$MH(H_2O)^+$																	
M_2H^+	117.16	0.52	145.22	0.524	173.26	0.747	257.42	0.838	$MH(H_2O)_4^+$	133.11	0.709	146.14	0.699	160.16	0.704	211.02	0.698
M_3H^+	175.24	0.733	217.33	0.768	259.39	0.887	385.63	1.096	$M_2H(H_2O)_4^+$	186.11	0.880						
M_4H^+	233.32	0.797	289.44	0.841	345.52	1.079	513.84	1.395	$M_3H(H_2O)_4^+$	174.22	1.05						
M_5H^+	291.4	0.895	361.55	1.034	431.65	1.384	642.05	1.622	$M_4H(H_2O)_4^+$	254.33	1.170						
M_6H^+	349.48	1.034	433.66	1.124	517.78	1.426			$M_5H(H_2O)_4^+$	330.44	1.296						
M_7H^+	407.56	1.106	505.77	1.365													
M_8H^+	465.64	1.212	577.88	1.494													
M_9H^+	523.72	1.297															

Compounds	Ethanol		1-propanol		Isopropanol		1-butanol		1-pentanol		1-heptanol	
	mass (amu)	1/Zo (Vs/cm^2)	mass (amu)	1/Zo (Vs/cm^2)	mass (amu)	1/Zo (Vs/cm^2)	mass (amu)	1/Zo (Vs/cm^2)	mass (amu)	1/Zo (Vs/cm^2)	mass (amu)	1/Zo (Vs/cm^2)
M^+	46.07	0.31	60.1	0.328	60.1	0.333	74.12	0.329	88.15	0.333	116.88	0.353
$MH(H_2O)^+$	65.07	0.497	79.1	0.507	79.1	0.508	93.12	0.510	107.15	0.513	135.88	0.519
M_2H^+	93.14	0.640	121.2	0.648	121.2	0.648	149.24	0.658	177.3	0.64919	234.76	0.644
M_3H^+	139.21	0.682	181.3	0.689	181.3	0.689	223.36	0.699	265.45	0.70027	351.64	0.699
M_4H^+	185.28	0.800	241.4	0.808	241.4	0.83	297.48	0.81	353.6	0.81026	468.52	0.814
M_5H^+	231.35	0.899	301.5	1.023	301.5	1.027	371.6	1.03	441.75	0.87303	585.4	0.938
M_6H^+	277.42		361.6	1.256	361.6	1.267	445.72	1.273	529.9	1.03206	702.28	1.093
M_7H^+	323.49	1.01475	421.7	1.349	421.7	1.364	519.84	1.371	618.05	1.27737	819.16	1.235
M_8H^+	369.56	1.241	481.8	1.433	481.8	1.435	593.96	1.445	706.2	1.379	936.04	1.369
M_9H^+	415.63	1.338										

M_5H^+ *versus* the molecular mass of the corresponding ketone (M). The three series in the graph show similar behaviour: a linear decreasing trend with mass for the ketones studied (acetone, 2-butanone, 2-pentanone and 2-octanone). In addition, it can be observed that the bigger the species the lower the slope exhibited in the linear trend.

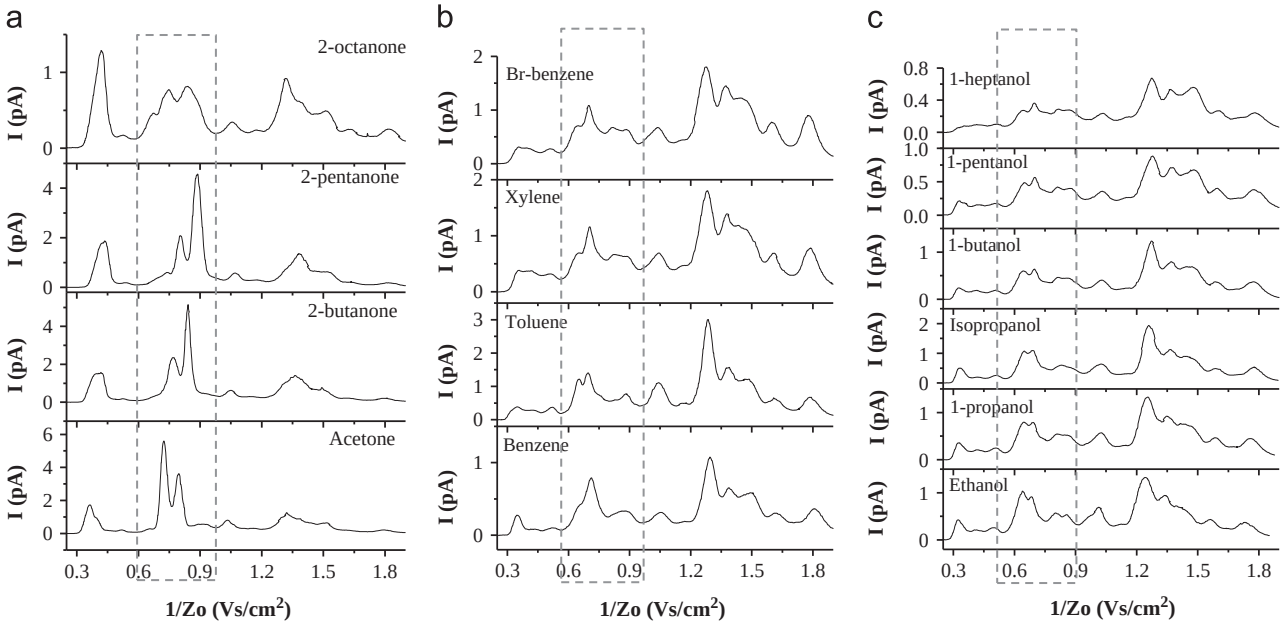

Fig. 6. Mobility spectra for three different families of compounds measured at 90 °C (a) Ketones, (b) Aromatic compounds and (c) Alcohols. The different square box highlighted the regions of the spectrum where the mobility for compounds helps to differentiate the different molecules in study.

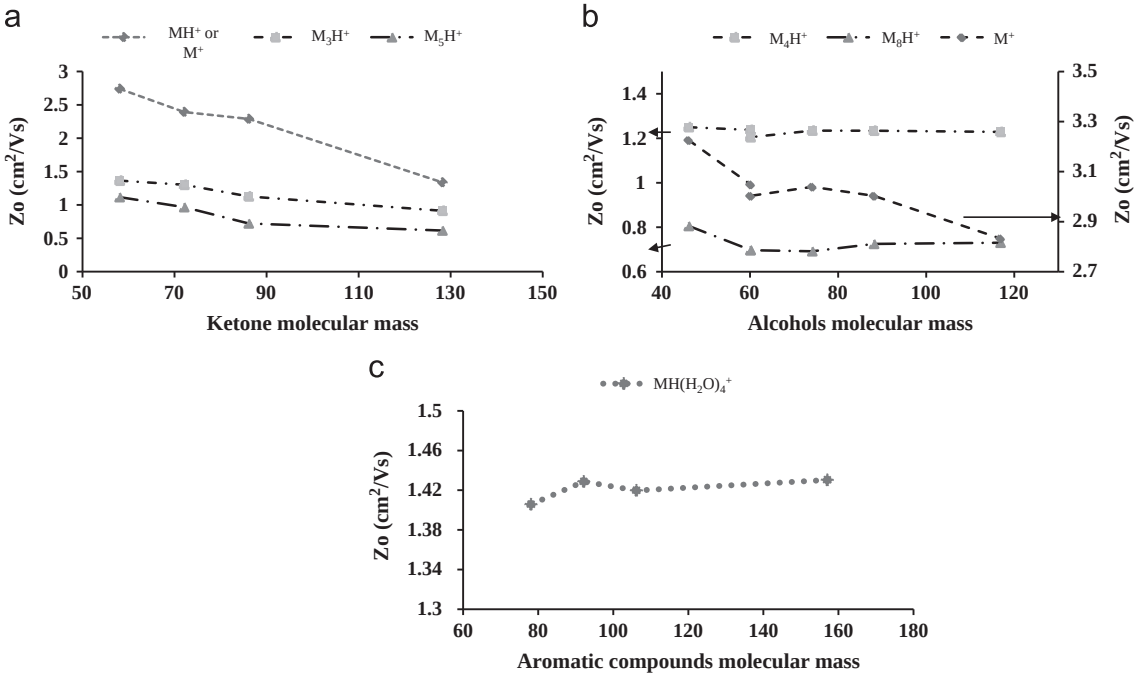

Fig. 7. Correlation between the reduced mobility (Zo) and the molecular mass for different ions detected of three different families of organic compounds: (a) Ketones, (b) Aromatic compounds and (c) Alcohols using the 10.6 eV UV–HRIMS.

In the case of alcohols (see Fig. 7b), a decreasing trend was again obtained for all alcoholic compounds studied. In this case, mobility and mass are correlated for the M^+ species.

Two different isomers were used (1-propanol and isopropanol, molecular mass 60.1 g/mol) for the alcohols study. The HRIMS instrument allowed to differentiating the 1-propanol and the isopropanol. Fig. 7b shows that, although for M_4H^+ and M_8H^+ the isomers could not be discriminated, M^+ mobility reveals differences between the primary alcohol (1-propanol) and the secondary alcohol (isopropanol).

Finally, Fig. 7c shows the mobility trend for the aromatic species ($MH(H_2O)_4^+$) *versus* the molecular mass of the corresponding aromatic compound. As can be seen, for these compounds the mobilities do not show the decreasing behaviour observed for the other families of VOCs. It was observed that the mobility of toluene and benzene are rather similar. It appears that aromatic compounds represent a special group of compounds with different rules to predict the mass/mobility correlation. Perhaps, other factors such as proton affinity, functional groups reactivity, or different possibility of coordination of the water clusters could influence the mobility of this family of compounds.

4. Conclusions

VOCs of different chemical families have been used for the characterization of a new instrumentation based on electrical mobility, an HRIMS. The differential mobility analyser follows the normal expected behaviour in terms of mobility when the temperature and the moisture present in the circuit of the instrument were investigated (lowering mobility, amplified signals and increased resolution).

Ion assignment studies have been performed for the different peaks found in the ion mobility spectra generated with a UV-lamp and detected with an ion counter for VOCs. The modified Millikan approximation added to Chem3D simulations allowed to carry out the identification of species detected using the HRIMS. Depending on the VOCs chemical family, the ionic species observed are different. A functional group with a strong proton affinity increases the possibility of forming aggregates during ionization, as it was observed with the ketones and the alcohols. The special behaviour of the aromatic species indicates that this is a family of compounds where more studies would be welcome. Finally, it should be highlighted that it would be most interesting to achieve direct ion identification with a mass spectrometer coupled to the HRIMS; this will be the goal of future research in our laboratory.

Acknowledgements

Financial support from the Gobierno del Principado de Asturias (PCTI Asturias) co-financed by “Eje prioritario 1 of FEDER program” through projects Ref.: PC10-59C1 and PC10-59C2 is gratefully acknowledged. RAMEM would like to acknowledge GANS project under Eurostars program.

References

[1] S. Armenta, M. Alcala, M. Blanco, Anal. Chim. Acta. 703 (2011) 114–123.
[2] G.A. Eiceman, Z. Karpas, Ion Mobility Spectrometry, 2nd edition, Taylor & Francis Group, Florida, 2005.
[3] J.M. Dilger, S.J. Valentine, M.S. Glover, M.A. Ewing, D.E. Clemmer, Int. J. Mass Spectrom. 332 (2012) 35–45.
[4] I. Márquez-Sillero, E. Aguilera-Herrador, S. Cárdenas, M. Valcárcel, TrAC-Trend Anal. Chem. 30 (2011) 677–690.
[5] K.M. Roscioli, X. Zhang, S.X. Li, G.H. Goetz, G. Cheng, Z. Zhang, W.F. Siems, H.H. Hill Jr., Int. J. Mass Spectrom. 336 (2013) 27–36.
[6] E. Ramiro, F. Ramiro, M. Sanchez, J.A. Lazcano, J.M. De Juan, J. Fernández de la Mora, J. Aerosol Sci. 34 (2003) S915–S916.
[7] J.P. Santos, E. Hontañón, E. Ramiro, M. Alonso, Atmos. Chem. Phys. 9 (2009) 2419–2429.
[8] R. Saleh, A. Shihadeh, A. Khlystov, J. Aerosol Sci. 40 (2009) 1019–1029.
[9] P. Kallinger, V.U. Weiss, A. Lehner, G. Allmaier, W.W. Szymanski, Particuology 11 (2013) 14–19.
[10] P. Intra, N. Tippayawong, Songklanakarin J. Sci. Technol. 2 (2008) 243–256.
[11] J. Fernandez de la Mora, L. de Juan, T. Eichler, J. Rosell, Trends Anal. Chem. 17 (1998) 328–338.
[12] C. Larriba, C.J. Hogan Jr., M. Attoui, R. Borrajo, J. Fernández García, J. Fernandez de la Mora, Aerosol. Sci. Tech. 45 (2011) 453–467.
[13] H. Tammet, J. Aerosol Sci. 26 (1995) 459–475.
[14] B.K. Ku, J. Fernandez de la Mora, Aerosol. Sci. Tech. 43 (2009) 241–249.
[15] S. Ude, F.J. Fernandez de la Mora, J. Aerosol. Sci. 36 (2005) 1224–1237.
[16] R. Guevremont, J. Chrom. A 1058 (2004) 3–19.
[17] V. Pomareda, S. Lopez-Vidal, D. Calvo, A. Pardo, S. Marco, Analyst 139 (2013) 3514.
[18] Ion mobility mass spectrometry: the next five years, Owlstone, 2013.
[19] M. Tabrizchi, Talanta 62 (2004) 65–70.
[20] E.V. Krylov, S.L. Coy, Erkinjon G. Nazarov, Int. J. Mass Spectrom. 279 (2009) 119–125.
[21] W.F. Siems, C. Wu, E.E. Tarver, H.H. Hill Jr., P.R. Larsen, D.G. McMinn, Anal. Chem. 66 (1994) 4195–4201.
[22] H. Borsdorf, T. Mayer, Talanta 101 (2012) 17–23.
[23] B.K. Ku, J. Fernandez de la Mora, J. Phys. Chem. B 108 (2004) 14915–14923.
[24] G.A. Eiceman, E.G. Nazarov, J.A. Stone, Anal. Chim. Acta 493 (2003) 185–194.
[25] M. Prakash, K. Gopal Samy, V. Subramanian, J. Phys. Chem. A 113 (2009) 13845–13852.
[26] N.L. Allinger, J. Am. Chem. Soc. 99 (1977) 8127–8134.